

See discussions, stats, and author profiles for this publication at: <https://www.researchgate.net/publication/262023722>

Unit Cell Structure of Water–Filled Monoolein into Inverted Hexagonal (H-II) Mesophase Modeled by Molecular Dynamics

ARTICLE in THE JOURNAL OF PHYSICAL CHEMISTRY B · MAY 2014

Impact Factor: 3.3 · DOI: 10.1021/jp411138r · Source: PubMed

CITATIONS

3

READS

34

5 AUTHORS, INCLUDING:



Vesselin Lyudmilov Kolev

University of Southern California

19 PUBLICATIONS 226 CITATIONS

[SEE PROFILE](#)



Galia Madjarova

Sofia University "St. Kliment Ohridski"

24 PUBLICATIONS 253 CITATIONS

[SEE PROFILE](#)

Unit Cell Structure of Water-Filled Monoolein into Inverted Hexagonal (H_{II}) Mesophase Modeled by Molecular Dynamics

Vesselin L. Kolev,^{*,†,‡} Anela N. Ivanova,[§] Galia K. Madjarova,[§] Abraham Aserin,^{||} and Nissim Garti[⊥]

[†]The Wolfson Department of Chemical Engineering, Technion, Technion City, Haifa 32000, Israel

[‡]Department of Chemical Engineering, Faculty of Chemistry and Pharmacy, Sofia University “St. Kliment Ohridski”, 1 James Bourchier Boulevard, Sofia 1164, Bulgaria

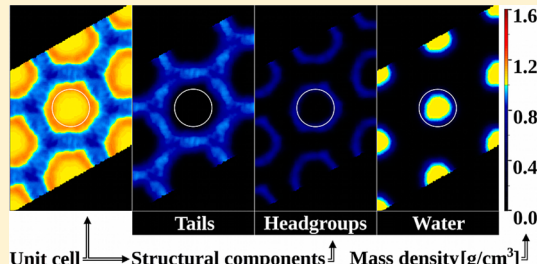
[§]Department of Physical Chemistry, Faculty of Chemistry and Pharmacy, Sofia University “St. Kliment Ohridski”, 1 James Bourchier Boulevard, Sofia 1164, Bulgaria

^{||}The Institute of Chemistry, The Hebrew University of Jerusalem, Edmond J. Safra Campus, Givat Ram, Jerusalem 91904, Israel

[⊥]The Ratner Chair in Chemistry, Casali Institute of Applied Chemistry, The Institute of Chemistry, The Hebrew University of Jerusalem, Edmond J. Safra Campus, Givat Ram, Jerusalem 91904, Israel

Supporting Information

ABSTRACT: The study investigates the unit cell structure of inverted hexagonal (H_{II}) mesophase composed of monoolein (1-monoolein, GMO) and water using atomistic molecular dynamics methods without imposing any restraints on lipid and water molecules. Statistically meaningful and very contrast images of the radial mass density distribution, scrutinizing also the separate components water, monoolein, the polar headgroups of the lipids, the double bond, and the termini of the hydrocarbon chain (the tail), are obtained. The lipid/water interface structure is analyzed based on the obtained water density distribution, on the estimated number of hydrogen bonds per monoolein headgroup, and on the headgroup–water radial distribution functions. The headgroup mass density distribution demonstrates hexagonal shape of the monoolein/water interface that is well-defined at higher water/monoolein ratios. Water interacts with the headgroups by forming a three-layer diffusive mass density distribution, and each layer’s shape is close to hexagonal, which is an indication of long-range structural interactions. It is found that the monoolein headgroups form a constant number of hydrogen bonds leaving an excessive amount of water molecules outside the first lipid coordination sphere. Furthermore, the quantity of water at the monoolein/water interface increases steadily upon extension of the unit cell, so the interface should have a very dynamic structure. Investigation of the hydrocarbon residues reveals high compression and well-expressed structuring of the tails. The tails form a very compressed and constrained structure of defined layers across the unit cell with properties corresponding to a more densely packed nonpolar liquid (oil). Due to the hexagonal shape the 2D packing frustration is constant and does not depend on the water content. All reported structural features are based on averaging of the atomic coordinates over the time-length of the simulation trajectories. That kind of processing allows the observation of the water/GMO interface shape and its stability and mobility at a time scale close to the ones of the intermolecular interactions.



1. INTRODUCTION

Lipid-based lyotropic liquid crystals (LLCs) are interesting and very promising novel lipid systems. They are a product of a self-assembly process involving lipid and water molecules. LLCs may be used as host systems for the crystallization of membrane proteins, for drug delivery, food applications, and inorganic synthesis.¹ Figure 1 represents one of the most fascinating LLC structures—the inverted hexagonal (H_{II}) mesophase, which is characterized by densely packed, water-filled lipid cylinders exhibiting two-dimensional hexagonal ordering. The monoolein-based H_{II} mesophases are extensively studied in terms of structural properties² and potential administration of bioactive macromolecules,³ such as lysozyme⁴ and insulin.⁵

The beginning of the characterization and theoretical investigations of the H_{II} mesophase structure dates back to 1962 when Luzzati and Husson published their structural model⁶ (see Figure 1a), which outlines the shape of the hexagonal unit cell (or simply “unit cell”) of the mesophase and its dimensions. The core idea of the model is to define a cylindrical lipid/water interface, which in turn confines the water content inside parallel cylinders immersed in the surrounding lipid (Figure 1a). This model can relate the spectroscopic measurements to the transversal dimensions of the unit cell. Leikin et al.⁷ extended the Luzzati and Husson

Received: November 12, 2013

Revised: April 17, 2014

Published: May 1, 2014

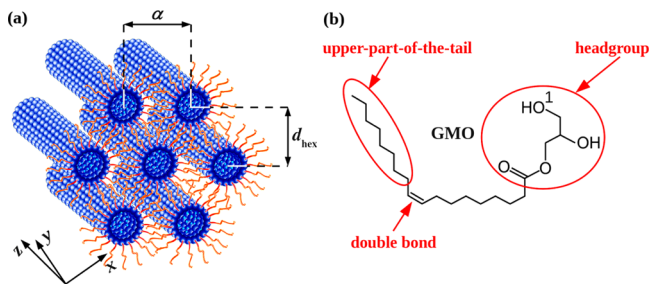


Figure 1. (a) Schematic representation of monoolein-based inverted hexagonal (H_{II}) mesophase and its parameters: α is the lattice parameter, d_{hex} is the first-order Bragg spacing measured by SAXS.² The water cylinders surrounded by lipid molecules are directed along the z -axis. (b) Chemical formula of 1-monoolein (glycerol monoleate, GMO) and its structural parts. The outermost hydroxyl oxygen atom is denoted with “1”.

idea by introducing cylindrical pivotal and neutral planes related to the elastic free energy of the system and its comparison to the osmotic work done by the osmotic stress. Similar extension was made by Templer et al.⁸ with an emphasis on the invariance of the pivotal area on isothermal bending.⁹

Based on a strong mechanical approach, Hamm and Kozlov proposed a new structural model known as the tilt model¹⁰ that provides a structural description not only of the H_{II} mesophase but also of the inverted amphiphilic mesophases in general. It also reflects the success of the experimental X-ray diffraction (XRD) reconstruction method.¹¹ Similar theoretical studies^{12–14} that are in accord with the tilt-model conclusion or explore its idea were published soon after.

Despite their mechanical adequacy, all listed structural methods cannot reveal structural details about lipid–lipid are water–lipid arrangement. One possibility to go beyond that and observe the local structure inside the unit cell is to predict the positions and interactions of the atoms by means of the methods of molecular dynamics (MD). A work by Marrink and Tieleman¹⁵ uses a united-atom force field and is focused on the phase transition between the inverted cubic and the inverted hexagonal phase but not on characterization of the two particular phases. The same group has performed two other studies^{16,17} employing either a united-atom or a coarse-grained MD computational protocol to study the self-assembly and/or phase transitions of lipid/water systems. In the latter, the inverted hexagonal phase of DOPE/water is described very briefly. There are two investigations representing the lipids at the coarse-grained level^{18,19} reporting phase diagrams, packing parameters and volume fractions of several phases, including the inverted hexagonal one. Other two reports^{20,21} study phase transitions involving the inverted hexagonal phase, which are due to external stimuli, e.g., a peptide or extra charge.

The structure dynamics inside the unit cell could be simulated with higher accuracy and in more details if fully atomistic MD simulations are carried out. But in order to ensure the success of the simulation procedure, there are at least two important problems that have to be solved in advance. The first is to find the optimal shape and size of the used unit cell. In a previous study²² we investigated the water dynamics within fixed GMO tubes and witnessed well-defined structuring of water in the proximity of the GMO heads. In order to verify that it was not an artifact due to the fixed lipid geometry or the restrained periodicity, the GMO dynamics is unrestrained in

the present work, and the hexagonal packing of the tubes is taken into account as well.

The second problem is the selection of the most appropriate descriptors of the structural dynamics inside the unit cell. One natural possibility is to track the mass distribution because it may characterize the inertia of atoms. For better scaling and comparing to experimental data, it is reasonable to depict and investigate the mass density distribution instead of the mass distribution itself.

The present study is an attempt to implement statistical analysis based on the data derived from MD trajectories for the investigation of the unit cell structure of a hexagonal inverted (H_{II}) mesophase composed of monoolein (GMO) and water. Monoolein (Figure 1b) is chosen because of the large scientific interest it has provoked recently.^{2,4,5} On the other hand, such a choice allows comparison of the obtained results to our previously derived semiquantitative ones.²² It should be stated clearly in advance that the H_{II} mesophases composed by mixing GMO and water (no cargo or admixtures) exists only at relatively high temperature (70°C)²³ that is inapplicable for biological systems. Nevertheless, the results are expected to be the basis for the future structural investigations at lower temperatures, especially in cases when some cargo is placed in the water channel, admixtures within the tails, or at the monoolein/water interface.

2. SIMULATION PROTOCOL AND PROCESSING OF THE RESULTS

To investigate theoretically the structure of the inverted hexagonal mesophase, a three-stage routine for simulation and data processing is applied: (i) preprocessing, (ii) MD simulation, and (iii) postprocessing (schematically shown in Figure 2).

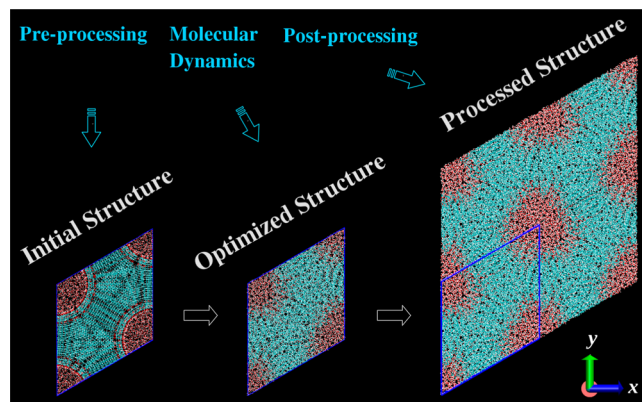


Figure 2. Schematic illustration of the simulation process.

The first two stages build and follow the equilibrium behavior of the self-assembled state of the system. The aim of (iii) is the description of the mass density distribution, based on the structure of the unit cell obtained by MD. The density averaging routine described in Section S2 in the Supporting Information largely guarantees a successful detection of the lipid/water interface shape, which is a novel numerical approach in this area. Also, it allows characterizing the influence of water content on the interface shape.

There is an additional treatment of one of the simulated systems—its unit cell with the equilibrated structure is replicated to build a “supercell”—a large (in size and number

Table 1. Source Experimental Data and the Calculated Numbers of Monoolein and Water Molecules in the Unit Cells^a

ϕ_w	α [Å]	R_w [Å]	N_w	N_l	$N_{w,hg}^*$	V_{cell} [Å ³]	V_w [Å ³]	V_l [Å ³]
0.17	50.53	10.94	615	156	3.94	110566.08	18806.33	91759.75
0.18	51.62	11.50	679	161	4.22	115382.43	20784.64	94597.79
0.19	52.69	12.06	747	166	4.50	120210.08	22861.87	97348.21
0.20	53.91	12.67	824	172	4.79	125842.54	25197.24	100645.30
0.21	55.16	13.27	904	178	5.08	131762.97	27646.16	104116.81
0.22	56.43	13.91	993	183	5.43	137906.43	30383.49	107522.94
0.23	57.63	14.51	1081	189	5.72	143827.05	33067.09	110759.96
0.24	58.85	15.15	1178	194	6.07	149971.29	36054.74	113916.55
0.25	60.25	15.83	1287	201	6.40	157195.62	39370.68	117824.94
0.26	61.53	16.47	1393	207	6.73	163912.77	42624.81	121287.97
0.27	63.01	17.19	1518	214	7.09	171942.30	46440.12	125502.18
0.28	64.47	17.92	1648	221	7.46	179979.64	50418.95	129560.68

^aColumns 1 and 2 contain the experimentally measured dependence $\alpha(\phi_w)$; R_w is the water cylinder radius (see eq 5); N_l and N_w are the calculated numbers of monoolein and water molecules that have to be placed inside the unit cell (Section S1 in the Supporting Information); $N_{w,hg}^*$ is the ratio N_w/N_l ; V_{cell} is the volume of the unit cell; and V_l and V_w are the partial volumes of monoolein and water in the unit cell, where $V_{cell} = V_l + V_w$ (Section S1 in the Supporting Information). The densities of monoolein and water – ρ_l and ρ_w , are taken at $t = 70^\circ\text{C}$ (at 70°C : $\rho_l = 1.0097 \text{ g/cm}^3$, $\rho_w = 0.9778 \text{ g/cm}^3$), and the length of the unit cell is set to $l = 50 \text{ \AA}$. Here ρ_l is calculated by using eq. S.6 in Section S1 of the Supporting Information, and ρ_w is a result of a spline interpolation of experimental data.

of atoms) analogue of the unit cell with the same shape. Then the multiplicative structure is simulated with MD, and the resulting trajectory is processed statistically to draw the distribution of the lattice parameter.

2.1. Preprocessing. During the preprocessing stage, the input structure for the MD simulation is composed by using a simplification of Luzzati and Husson,⁶ so the composition of the unit cell for the MD simulation requires setting the shape of the periodic box and determination of the lipid and water content therein.

The lattice parameter of the H_{II} mesophase α (Figure 1a) defines the characteristic size of the unit cell in the plane of two-dimensional repetition of the structure and it is related to the first-order Bragg spacing, d_{hex} , measured experimentally by small-angle X-ray scattering (SAXS):

$$\alpha = \frac{2}{\sqrt{3}} d_{hex} \quad (1)$$

The geometrical approach of Luzzati and Husson proposes a relation between the cross-section area of the inverted hexagonal mesophase unit cell, σ , and the lattice parameter:

$$\sigma = \frac{\alpha^2 \sqrt{3}}{2} \quad (2)$$

Thereby, the cross-section areas of water and lipid, σ_w and σ_l , are

$$\sigma_w = \varphi_w \sigma \quad (3)$$

$$\sigma_l = (1 - \varphi_w) \sigma \quad (4)$$

where φ_w is the water volume fraction. As an important corollary of eq 3, the curvature of the water channel is related to σ_w :

$$R_w = \alpha \sqrt{\frac{\sqrt{3}}{2\pi} \varphi_w} \quad (5)$$

where R_w is the radius of the water cylinder.²⁴ Despite the fact that eq 5 is not part of Luzzati and Husson's original publication, R_w could be derived by applying their model and it is recognized as a parameter of the lipid/water interface shape.

To estimate the unit cell (periodic box) sizes, experimentally measured pairs of data $[\phi_w, \alpha]$ are needed. For each pair $[\phi_w, \alpha]$, the sizes of the unit cell, the quantity of water and GMO inside, and the initial positions of the molecules (the structure) can be calculated by following the routines in Section S1 in the Supporting Information. This nonstandard procedure usually is not available in the MD software, but it is mandatory if the initial distribution of water and GMO within the unit cell needs to be homogeneous. Note that an additional parameter has to be introduced arbitrarily to make the volume of the unit cell finite (Section S1 in the Supporting Information): the longitudinal size (the length) of the cell, l . The used numerical values of l should be large enough to minimize the mass density estimation error that occurs due to the fact that the number of monoolein and water molecules in Table 1 is always an integer. On the other hand, l must be small enough to render the simulations computationally efficient. $l = 50 \text{ \AA}$ is used in the current study.

Table 1 shows the outcome from the application of the formulas in Section S1 in the Supporting Information, namely, the estimated monoolein and water content in the unit cell for 12 experimentally measured⁶ pairs $[\phi_w, \alpha]$, which allows tracing the effect of the water cylinder thickness on the lipid–water interactions. Figure 3 illustrates the unit cell dimensions and initial positions of the molecules (the initial structure of the H_{II} mesophase).

2.2. Molecular Dynamics Simulation. The MD simulations are done with the program package GROMACS 4.5.5.²⁵ The lipid parametrization of the force field CHARMM27^{25,26} is used for the GMO molecules, and the TIP3P model^{27,28} is employed for water. The simulation box coincides with the hexagonal inverted mesophase unit cell (whose dimensions are defined by means of the procedure described in Section S1 in the Supporting Information), i.e., a rhombic unit cell to which hexagonal periodic boundary conditions are applied. The formulas for estimation of the box vectors for each of the unit cells are presented in Table SI in the Supporting Information in Gromos87 file format.²⁹

During the minimization stage, position restraints (harmonic restraining potential with $k = 1000 \text{ kJ/mol}\cdot\text{nm}^2$ per atom) are imposed on the GMO molecules. The minimization of such a

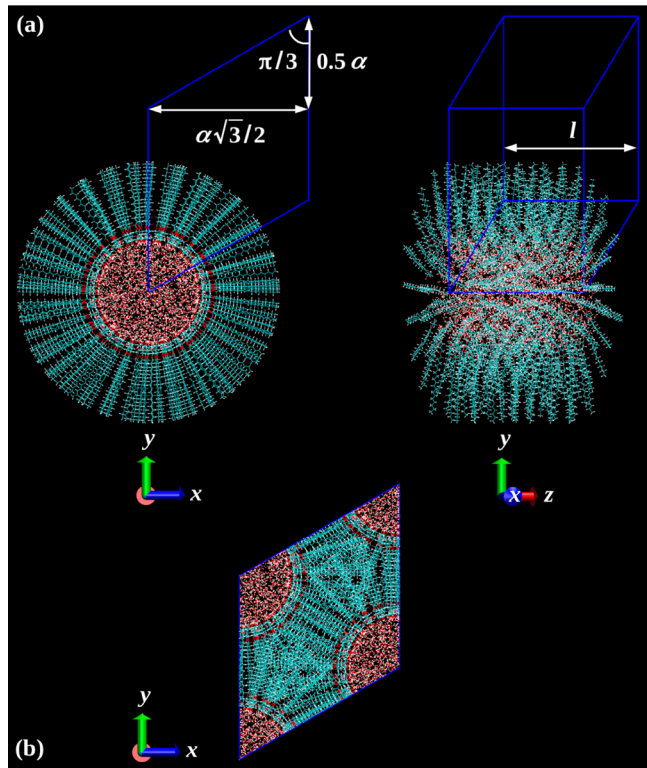


Figure 3. Starting homogeneous structure of the H_{II} mesophase inside the hexagonal periodic unit cell. Here (a) represents the sizes of the unit cell while (b) shows how the structure fits the cell.

crowded system was facilitated by the rational choice of the initial topology of the inverted hexagonal mesophase described in Section 2.1. The proposed homogeneous distribution of the GMO molecules combined with rotation of the monoolein tails allowed the structure to be minimized, avoiding undesirable cramming of the monoolein molecules.

The minimized structure is heated to the temperature (70°C) at which samples of H_{II} mesophase are investigated experimentally. The initial velocities of the atoms are generated from the Maxwell–Boltzmann distribution at 2 K. The v -rescale algorithm is used³⁰ to control the temperature. The position restraints on the monoolein atoms are preserved during heating. After achieving the desired temperature within 500 ps, the restraints on GMO are relieved, and the system is allowed to relax for 1 ns at 70°C .

Then the equilibrium dynamics of the structure is studied in the production stage of 20 ns length. Electrostatic interactions are evaluated by the PME method³¹ with a cutoff of 14 Å (a switching function turned on at 12 Å) on the direct part of the sums. A switched cutoff of 12 Å, the switching function turned on at 10 Å, is applied for the nonbonded interactions. LINCS³² and SETTLE³³ are used for fixing the length of the H-containing bonds of GMO and water, respectively. Most of the MD simulations are carried out in NVT ensemble. The Berendsen barostat controls the pressure in some additional NPT simulations (see Section 3.4). The MD trajectories are subject to statistical analysis on frames extracted at intervals of 1 ps to obtain the average properties reported below.

2.3. Postprocessing. The postprocessing stage provides the mass density distribution across the unit cell using the 12 20 ns long MD trajectories. The last 10 ns of each trajectory are decomposed into 10 000 consecutive frames, saved in

Gromos87 file format (one file per frame), and analyzed by the routine described in Section S2 in the Supporting Information.

In addition, the subdistributions of the structural components: water, GMO, GMO headgroups, double bond in the GMO chain, and the upper part of the chain tail (see also Figure 1), are obtained by applying the routine from Section S2 in the Supporting Information to each of them separately.

For creating the supercell mentioned above, the unit cell with one tube with $\alpha = 64.47 \text{ \AA}$ is used. It contains 1648 water and 221 GMO molecules. The maximum possible number of repetitions (within the presentation format of the used software package) of the unit cell that reproduces the shape of the parent cell is 49 (7×7). Figure S5 in the Supporting Information shows the constructed 7×7 supercell.

3. RESULTS AND DISCUSSION

In order to illustrate the influence of the GMO cylinder size, the results for three of the studied systems are presented below: the smallest and the largest one and a tube with intermediate diameter.

3.1. Mass Density Distribution Maps. Figures 4–6 show the mass density distribution plotted as color maps. The colors used for mapping the density values (see the color scale on the right of each picture) are selected in a way that visualizes at least 95–97% of the distribution. The color transition point is near the bulk water density (1.00 g/cm^3). Such a transition is introduced to allow a sensitive subtraction of the water density from the total density.

The total distribution of the mass density (Figure 4a) is a nice illustration of the internal structure of the unit cell. It outlines predominantly hexagonal shape of the tube lipid surface, which is in accordance with the prediction of the tilt model.¹⁰ It should be noted that placing the model system in hexagonal periodic boundary conditions in order to comply with the experimentally known arrangement of the GMO cylinders does not guarantee hexagonal ordering of the lipids within the cylinder, and, thus, this is not an artifact of the PBC applied. The density minimum is located near the vertices of the hexagonal structure formed by the tails. The densest region (up to 1.2 g/cm^3) is the one formed by the hydrated lipid headgroups. The shape and overall density distribution pattern are insensitive to the tube diameter. As could be expected, the total density of all parts of the system decreases slightly upon tube diameter increase. The hexagonal shape of the channel is well discernible even in the smallest model system, but the higher the water content, the more pronounced the hexagonal shape. This is well-illustrated by plotting the headgroup density distribution in Figure 5.

Figure 4b shows how the water density is distributed across the unit cell. Here the distribution shape far from the center (colored in deep blue) matches the same hexagonal structure. That external diffuse part of the distribution corresponds well to the intersection of water and monoolein, i.e., to the water/monoolein interface. Thereby, it also confirms the tilt model and the coarse-grained MD predictions. The atomistic details allow further discrimination, namely, that the radial profile of the water density features three distinct subshells. Close to the center of the tube the water density is similar to the bulk value (even in the narrowest cylinder); a relatively thin interfacial layer with lower density follows. It then transforms abruptly into the more diffuse layer, which can be attributed to the water molecules protruding among the lipid headgroups. The

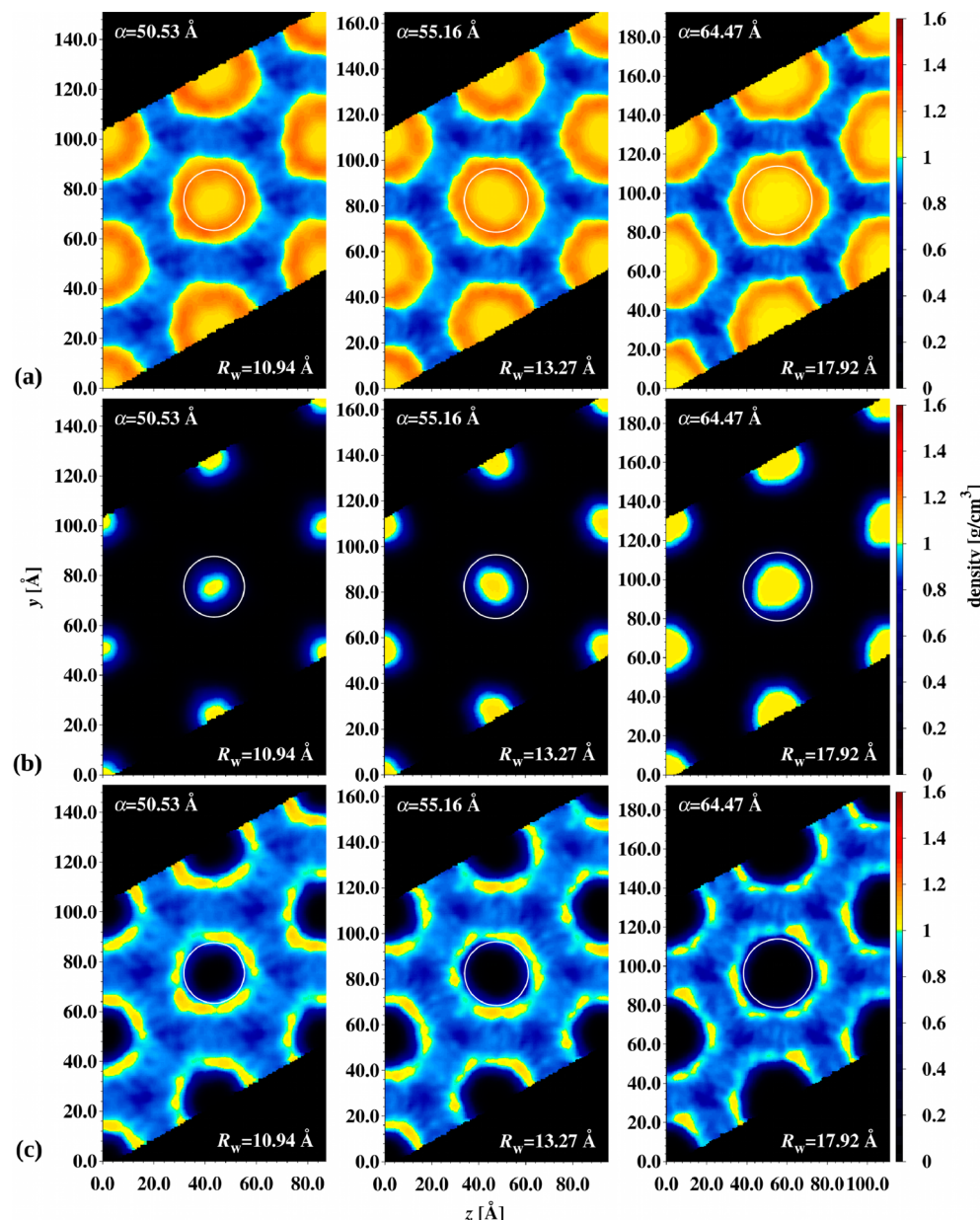


Figure 4. Total mass density distribution (a), and the mass density distribution of water (b) and monoolein (c) as a function of the amount of water in the GMO cylinders; the white circle is a guide for the eye, designating Luzzati and Husson's idea of a water cylinder.

existence of such distinct density regions implies that the water structure is strongly affected by the lipid headgroups and also that different microstructuring of water in the three subshells could be expected.

The distribution of the monoolein molecules (Figure 4c) shows that the lipid density is highly frustrated around the water channel. The pronounced inhomogeneity of the density distribution in the region of the headgroups, combined with the tails' density depletion at the vertices mentioned above, signifies clustering of the GMO molecules along the hexagon edges.

Analysis of the maps in Figure 6 shows interesting results. There is evident structuring of the lipid tails (Figure 6a). Decomposition of the analysis for the upper part of the tails (Figure 6b) and for the double bond (Figure 6c) reveals that it is the double bond in the tails that is very well constrained. The constraints are so tight that these bonds form planes inside the

unit cell structure. It is interesting that the ordering does not weaken even where the total mass density is low.

3.2. Radial Distribution Functions. In order to refine the structural elucidation of the studied systems, three radial distribution functions (RDF) are generated: (i) between the terminal hydroxyl oxygen from the GMO headgroups (O1 in Figure 1b) and the water oxygen (OW) atoms, (ii) between the centers of mass (COM) of the double bonds, and (iii) between the COMs of the upper parts of the lipid tails. The curves for the three representative models are shown in Figure 7.

The water structuring observed in our previous study²² is also preserved when the lipid geometry is relaxed. There are two well-shaped peaks in the O1-OW RDF (Figure 7a), which is characteristic of the experimental liquid water structure at room temperature.³⁴ On the other hand, the TIP3P water model is known to lack the peak for second neighbors at this temperature.^{27,28} Hence, the fact that the second maximum

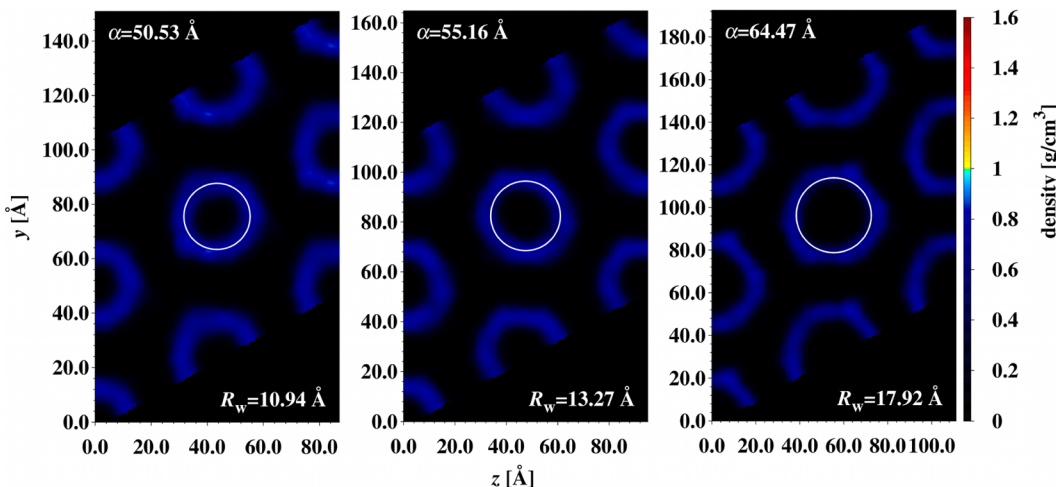


Figure 5. Mass density distribution of the monoolein headgroups as a function of the size of the GMO cylinders. See Figure 1b for the definition of the headgroup structure in the monoolein molecule. Here the white circle is a guide to the eye, which designates Luzzati and Hussons' idea of a water cylinder.

exists in our models at 70 °C is a clear indication of water immobilization in the vicinity of the GMO headgroups as discussed above for the water density maps. The main features of the RDF profiles do not change upon tube diameter increase but the maximum of the first neighbors decreases in intensity at the expense of faster reach of the homogeneous density.

The structuring of the lipid tails is very well-expressed in the two RDFs (Figure 7b and c). Both the double bond and the upper part of the tails have three well-shaped maxima, which is indicative of a definite pattern of packing of the lipids. The ratio between the distances of the first two maxima is 1.88, which is slightly larger than that for hexagonal lattice. The RDF curves for the lipid tails in the two smaller tubes practically coincide, while in the largest system a slightly higher share of the molecules participates in the structuring.

3.3. Headgroups Hydration. Another interesting aspect here is the quantity of water molecules hydrating the headgroups in the different GMO tubes. Its estimation might be based on the calculation of the number of water molecules per lipid head, $N_{w,hg}$ (the process is explained in Section 2.3) on the one hand, and on the number of hydrogen bonds formed between the lipid headgroups and the water molecules on the other.

The average number of hydrogen bonds in the 12 tubes is summarized in Table 2. The length distribution in the three illustrative systems is presented in Figures 8 and S7.

The profile of the length distribution (Figure 8) is virtually identical for all tubes, irrespective of their diameter, which means that the hydrogen-bonding pattern is already established in the smallest channel and is not affected by the tube growth. The most populated H-bond length is ~1.875 Å, corresponding to strong hydrogen bonding of water to the GMO headgroups. The constant number of $\sim 3 \pm 0.1$ hydrogen bonds per lipid (Table 2) in all tubes indicates that the hydrogen bonding capacity is not spatially restrained in the narrowest tube and that it is insensitive to the tube diameter.

There is another interesting feature of the hydrogen bond length distribution depicted in Figures 8 and S7. Independently of the tube diameter, the maximum is irregularly shaped, and the most expressed peak is at 1.875 Å. It may be assumed that a second maximum centered at 2.025 Å exists. However, the overlap is too substantial to claim that this distribution of the

bond lengths is indicative of different type of hydrogen bonding of the oxygen atoms in the headgroup and the surrounding water molecules. In principle, the type of hydrogen bonding may be discriminated by computational vibrational analysis.³³ However, this procedure is inapplicable within the current computational setup and was therefore substituted by a more detailed inspection of the hydrogen bonds formed by the separate residues (hydroxyl group, carbonyl oxygen, ester oxygen) with water. It shows that all kinds of bonds span the entire distance region with slight preference for shorter bond lengths of the carbonyl oxygen atom from the carboxyl group.

Figure 9 depicts the results for the total number of water molecules per lipid headgroup derived for each system described in Table 1. In addition, a correlation diagram is plotted there to check whether the ratio between the number of water molecules and GMO headgroups in the layer formed by the headgroups is similar to the one between the total number of water and GMO molecules in the unit cell. To make the ratios compatible, each value is divided by the respective observed value in the tube with the largest diameter (maximum observed value). The maximum observed value of the number of water molecules per GMO headgroup, $N_{w,hg}(\max)$, in Figure 9 is 16.70. As for the maximum observed value of the total number of water molecules per GMO, $N_{w,hg}^*(\max)$, it is located in the last row of Table 1 (column 6).

The number of water molecules per GMO headgroup, $N_{w,hg}$, plotted in Figure 9 as a function of the lattice parameter α , and statistically defined in Section S3 in the Supporting Information (eq S.11), is not an explicit function of the number of hydrogen bonds established by the headgroup with the surrounding water molecules. It is mostly a statistical estimator of the quantity of water hydrating the GMO headgroups. The fact that $N_{w,hg}$ is not a constant and strongly depends on α means that it is not related only to the number of the established hydrogen bonds. On the contrary, such a dependence is most probably an indicator that there is a large quantity of water molecules not bonded directly to the GMO headgroups and their equilibrium dynamics contributes largely to $N_{w,hg}$. This hypothesis is supported by the correlation diagram in Figure 9. Since the slope of the linear dependency is almost 1.0 and its standard deviation is less than 1%, the quantity of water in the headgroups layer should be an *explicit* function of the total

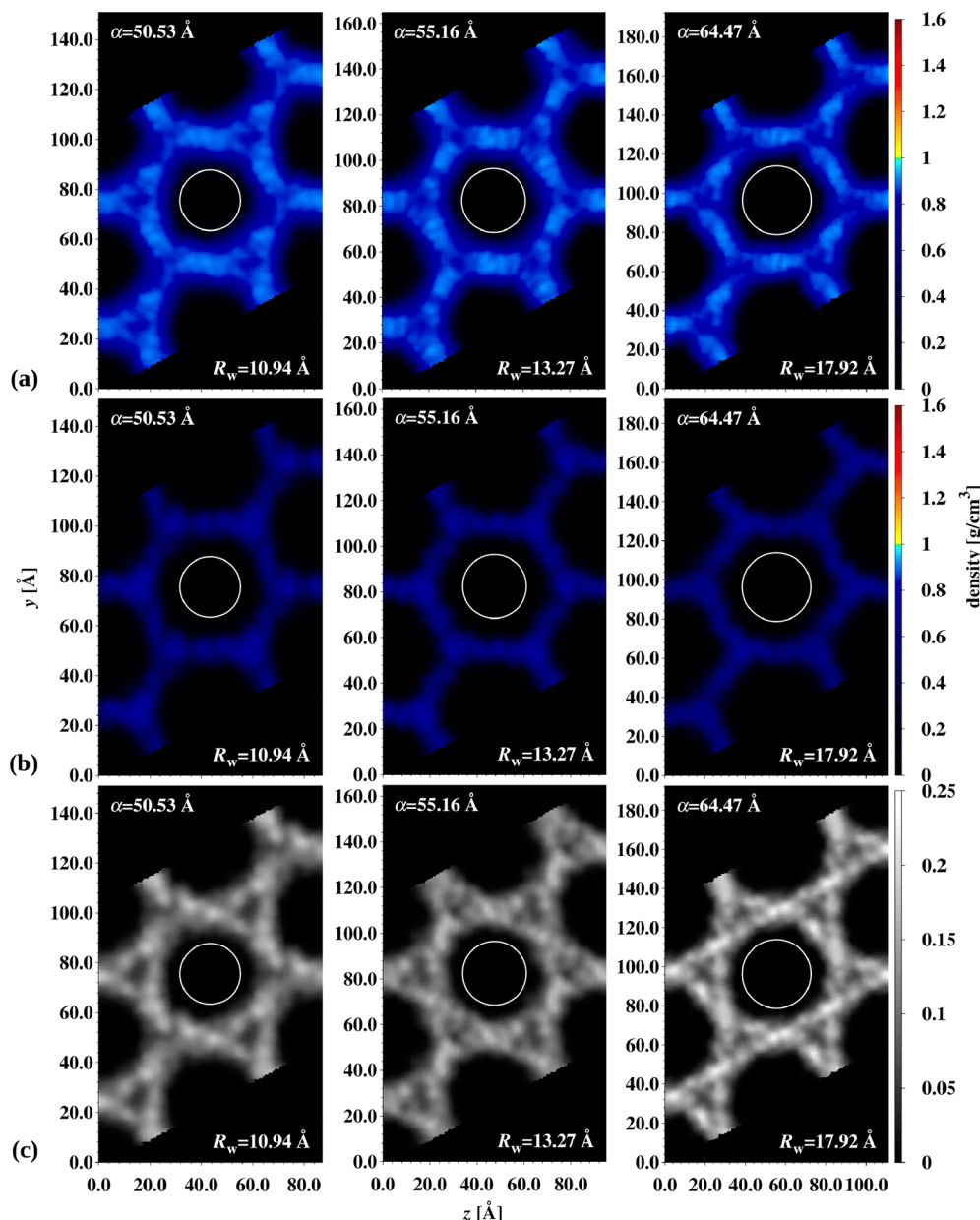


Figure 6. Mass density distribution of monoolein tails (a), their upper-part (b), and double bond (c) in GMO cylinders with increasing diameter. See also Figure 1b. The white circle is a guide for the eye, designating Luzzati and Husson's idea of a water cylinder.

quantity of water inside the H_{II} mesophase unit cell. Therefore, $N_{w,hg}$ is related strongly to N_w and thereby there is a significant quantity of non-hydrogen-bonded water molecules between the GMO headgroups that is correlated mostly to the equilibrium dynamics and the corresponding flux of water to and from the headgroup layer. The fact that $N_{w,hg}$ grows with increase of the tube diameter is an indication that, in all studied systems, the hydration sphere of the GMO headgroups has not reached saturation.

3.4. NVT vs NPT. To check whether the reported structural effects are an artifact of the NVT ensemble, additional simulations with an NPT ensemble were performed according to protocols described in Section 2. That change of the ensemble causes $\approx 13\%$ expansion of the unit cell volume, which reflects the elasticity of the lipid molecules. Such an expansion corresponds to 5% increase of α and l , which is close to the experimental uncertainty of 1%. Despite that, the

structural features reported in Section 3.1 remain unchanged. Also, the replacement of the statistical ensemble does not significantly alter the hydration of the headgroups discussed in Section 3.3 (less than 2% decrease). In fact, the only visible effect of the ensemble replacement is some growth in the sizes of the images previously plotted for NVT in Figures 4–6, due to the higher value of α .

3.5. Assessing the Approach Adequacy. The statistical distribution of the lattice parameter, α , could specify whether it is possible to describe in general the properties of an infinite H_{II} mesophase structure by using just one “tube” put into a finite unit cell and with PBC applied. If a “supercell” containing more than one GMO tube (described above) is subject to MD simulation and its structure is virtually a repetition of the original unit cell structure, then the small model with one tube could be considered adequate. The estimated distribution of α in the supercell corresponding to the last system in Table 1 has

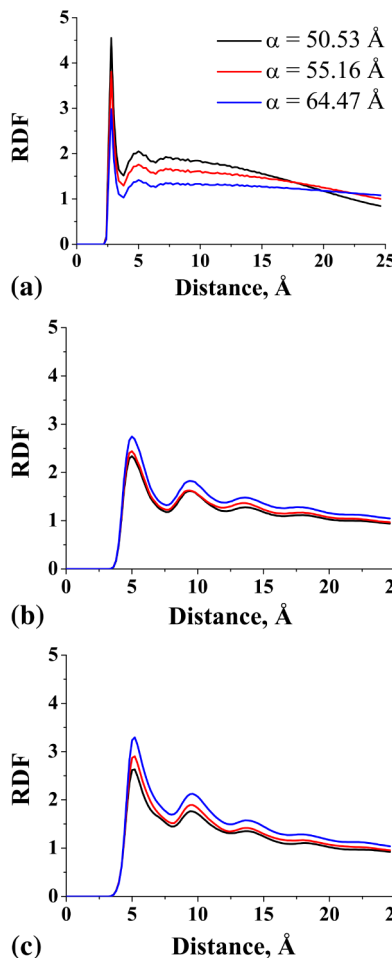


Figure 7. Radial distribution function of the GMO hydroxyl oxygen–water oxygen atoms (a), the COMs of the double bond (b), and the COMs of the upper part (c) of the lipid tails as a function of the tube diameter. The hydroxyl oxygen atom in the monoolein molecule is marked with “1” in Figure 1b.

Table 2. Average Number (With Standard Deviations) $N_{\text{avg}}(\text{total})$ of Hydrogen Bonds between the Lipid Headgroups and the Water Molecules As a Function of the Water Tube Diameter R_w^a

$R_w [\text{\AA}]$	$N_{\text{avg}}(\text{total})$	$N_{\text{avg}}(\text{scaled})$
10.94	441.8 ± 17.6	2.8 ± 0.1
11.50	462.7 ± 19.6	2.9 ± 0.1
12.06	482.4 ± 19.2	2.9 ± 0.1
12.67	503.6 ± 20.4	2.9 ± 0.1
13.27	525.3 ± 20.1	3.0 ± 0.1
13.91	549.2 ± 21.8	3.0 ± 0.1
14.51	564.7 ± 21.1	3.0 ± 0.1
15.15	593.7 ± 22.8	3.1 ± 0.1
15.83	611.3 ± 22.2	3.0 ± 0.1
16.47	640.1 ± 24.8	3.1 ± 0.1
17.19	657.2 ± 24.1	3.1 ± 0.1
17.92	683.0 ± 24.0	3.1 ± 0.1

^aThe third column contains the average value scaled per lipid molecule $N_{\text{avg}}(\text{scaled})$.

an expectation value of 64.63 \AA , which is very close to the measured experimental lattice parameter (64.47 \AA). More details are presented in Section S4 in the Supporting

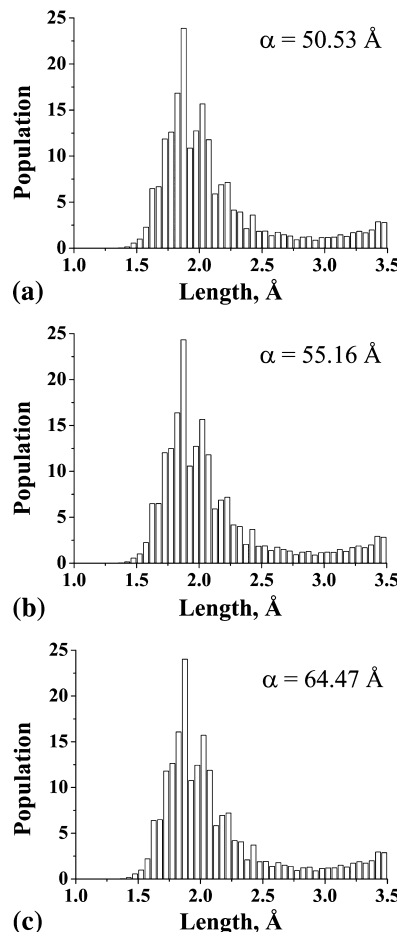


Figure 8. Distribution of headgroup–water hydrogen bond lengths as a function of the lattice parameter.

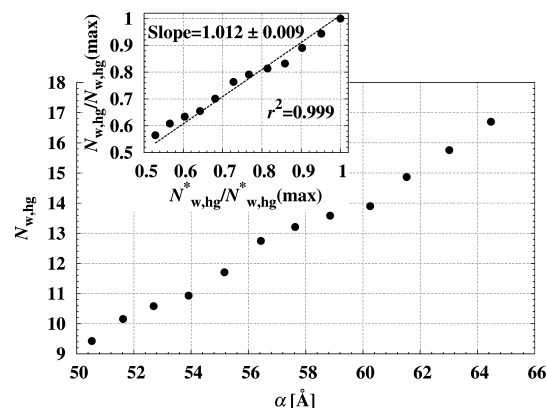


Figure 9. Estimated number of water molecules per GMO headgroup, $N_{w,hg}$, as a function of the lattice parameter of the H_{ll} mesophase unit cell, α . The inset shows the linear correlation between the reduced and the total ($N_{w,l}^*$) number of water molecules per GMO headgroup (the last is presented in Table 1). The reduction is made by dividing $N_{w,hg}$ and $N_{w,l}^*$ by the respective maximum observed values, denoted as $N_{w,hg}^{\text{(max)}}$ and $N_{w,l}^{\text{(max)}}$.

Information. The outcome of this test justifies the use of the small model.

3.6. 2D Packing Frustration Analysis. Several X-ray diffraction studies characterizing the H_{ll} mesophase of the lipid/water system report results where the shape of the interface varies from hexagonal to circular depending on the

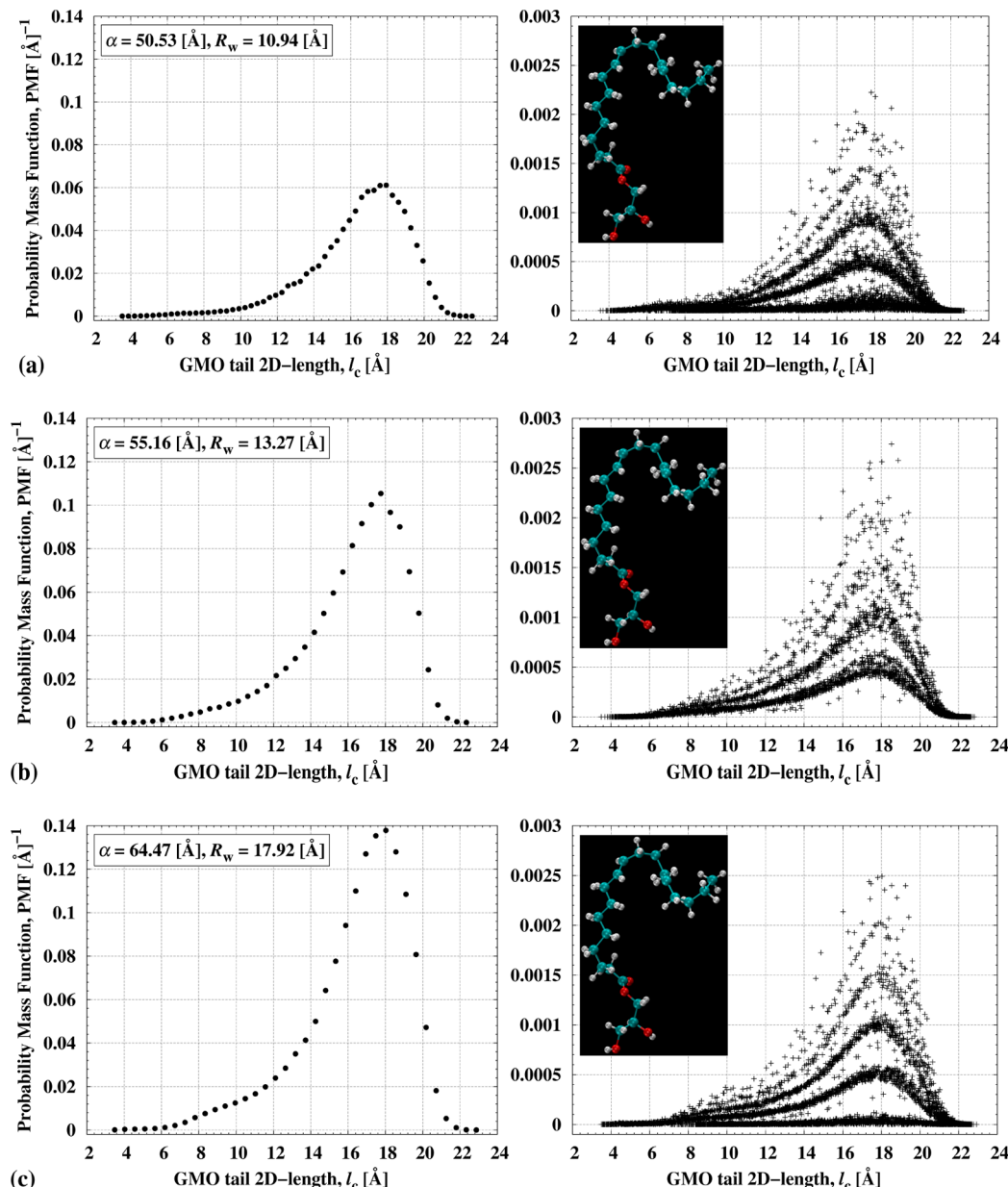


Figure 10. Probability mass function (PMF) of GMO tail 2D-length, l_c , for the H_{II} mesophases presented in Figures 4–6. The PMF plots on the left are obtained by separating the measured l_c values amid 100 bins, while the right ones are obtained at 16 000 bins. The inset presents a picture of the tail configuration of the GMO molecule the discrete l_c -distribution of which is mostly responsible for the formation of the observed PMF decomposition at 16 000 bins.

specificity of the lipids.^{36–38} This is indicative of some packing frustration caused by two counteracting driving forces: the spontaneous cylindrical curvature of a bending monolayer versus the hexagonal tight packing of 2D space.

In order to quantitatively investigate the packing frustration of GMO tails in the H_{II} mesophases presented in Figures 4–6, 10 000 frames out of each molecular dynamics trajectory were extracted. Then, the xy -coordinates of the atoms were examined, and the maximum 2D-length of the hydrocarbon tails of each GMO molecule, l_c , was calculated and stored into an array. Finally, the array content was separated into intervals (bins) and the corresponding probability mass functions (PMF) of GMO tails 2D-length were obtained and plotted in Figure 10. It is shown there that if the measured l_c is separated among a large set of narrow bins, all PMF plots are transformed

into a complex composition of several sub-PMFs. This phenomenon might be an indication that l_c is discretely distributed within a finite number of structural classes. Each of them may be defined as a set of GMO tails that share almost the same l_c and, hence, have similar (close) structural conformations. Also the analysis of the trajectories showed that due to the conformational dynamics of the hydrocarbon chains, every structural conformation may change its membership and migrate from one class to another. In Figure 10 there is a picture of the most populated structural conformation of the lipid tails that is a member of several structural classes and has large contribution to the formation of the sub-PMF structure. Of course, there are more tail conformations, but they are not shown because of their lower influence. The point density of each class in Figure 10 and the corresponding PMF

values might be used as an estimate of the class population, because it is related to the number of GMO molecules that passed through that particular class during the simulation. Note that the sub-PMF structure in Figure 10 does not change with the abscissa partitioning (varying the number of the bins). So, its appearance is unlikely to be related to an artifact brought in by the numerical methods involved into estimation of the chain lengths and their separation among the bins along the PMF abscissa.

The next task is to establish a quantitative connection between the 2D packing frustration phenomena and the PMF in Figure 10. In the classical H_{II} mesophase structural theory, the 2D packing frustration, Δl_c , is quantitatively connected to the difference between the maximum and minimum thickness of the lipid tails layer – $l_{c,max}$ and $l_{c,min}$:²

$$\Delta l_c = l_{c,max} - l_{c,min} \quad (6)$$

$$l_{c,min} = \frac{\alpha}{2} - R_w \quad (7)$$

$$l_{c,max} = \frac{\alpha}{\sqrt{3}} - R_w \quad (8)$$

However, since the shape of the water/GMO interface in our study deviates significantly from cylindrical, $l_{c,min}$ and $l_{c,max}$ should be extracted from the PMF (Figure 10). According to the properties of the PMF function, the value of l_c at the functional maximum is considered the most probable GMO tail length, and the lower and upper limits of its variance are estimations of $l_{c,min}$ and $l_{c,max}$. Table 3 contains $l_{c,min}$ and $l_{c,max}$ obtained by means of eqs 6,7,8 (the classical approach) and by this simple analysis of the PMF.

Table 3. Comparison between the Values of $l_{c,min}$, $l_{c,max}$, and Δl_c Estimated by Using the Classical Approach (Eqs 6, 7, and 8), and Numerical Analysis of PMF^a

α [Å] (Table 1)	R_w [Å] (eq 5)	classical approach (eqs 6,7,8)			this study (analyzing data in Figure 10)		
		$l_{c,min}$ [Å]	$l_{c,max}$ [Å]	Δl_c [Å]	$l_{c,min}$ [Å]	$l_{c,max}$ [Å]	Δl_c [Å]
50.53	10.94	14.33	18.23	3.90	15.85	19.94	4.09
55.16	13.27	14.31	18.68	4.37	15.84	20.02	4.18
64.47	17.92	14.31	19.30	4.99	16.18	20.18	4.00

^aThe numerical analysis is based on fitting the data in Figure 10 (left) with Chebyshev polynomials of 10th order and calculating $l_{c,min}$ and $l_{c,max}$ as the l_c values at the PMF points of inflection, which automatically defines Δl_c as the variance of the most probable value of l_c . Note that the values of Δl_c thus obtained and stored in the last column are statistically indistinguishable due to the fit error; so, their arithmetic average should be used as a general assessment of Δl_c in all the H_{II} mesophases investigated herein.

The results in Table 3 show that there is 2D packing frustration in our systems. It has constant magnitude that does not depend on the water content. Such a result is not unexpected since the hexagonal shape in Figure 6a correlates well with the idea of denser tails packing in radial directions. There, the lipid chains, being in a quasi-liquid state, tend to distribute uniformly in radial direction with respect to the hexagonal shape. Only at the hexagon vertices the local curvature there causes a “dilution” of the quasi-liquid of the lipid chains, which in turn decreases the local mass density in these regions, as seen in Figures 4a,c and 6a. Therefore, the

distance between two neighboring hexagon vertices should be related to the stability of H_{II} mesophases, because the larger the tube diameter, the longer the hexagon walls, and the weaker the necessity for lipid density redistribution will be. Therefore, the tails packing plays an essential role for the overall shape of the H_{II} mesophase interface.

4. CONCLUSIONS

A direct result of this study is the theoretical evaluation of the unit cell geometry of the monoolein/water inverted hexagonal mesophase at an atomic-level scale. One of the most essential findings is the mostly hexagonal shape of the monoolein/water interface, which is in accordance with the predictions of the mechanical tilt model and of coarse-grained MD simulations. Another important observation is the intensive dynamics of the water molecules located near and inside the water/lipid interface—only a small quantity of them participate in hydrogen bonds with the monoolein headgroups. The rest could be considered nonlipid-bonded, and their quantity depends almost linearly on the water/monoolein ratio. Such a fact might be interpreted as evidence that the nonbonded interactions (electrostatic, van der Waals), and not the lipid–water hydrogen bonding, define the shape of the monoolein/water interface.

Another conclusion is that the monoolein tails form a very compressed and regular internal structure (layer) inside the unit cell. Even well-shaped planes that participate in symmetrical structures of higher order are visible. Therefore, the layer formed by the monoolein tails might be considered a highly packed (structured) liquid because at the observed compressibility the tails seem to be self-dissolved. This is a somewhat expected result, since even the Luzzati and Husson⁶ structural model points to it. However, the existence of a hexagonal shape of the monoolein/water interface leads to much greater compressibility of the tails, especially at high water content. This might be essential for their role as bioactive cargo carriers.

An important part of the work is the development of a robust set of routines for constructing homogeneously distributed initial structure of the unit cell of the inverted hexagonal mesophase and for nonstandard analysis of the mass density distribution. The proposed procedure for construction of such heterophase unit cells with extremely nonstandard geometry has the potential for more general application. Moreover, the developed preprocessing procedure lowers the computational costs and shortens the simulation time. As a result, it enables the simulation of a relatively large number of model systems and straightforward extension of the unit cells.

The results prove that the mass density distribution maps generated by our protocol could be used as a reliable source of structural information. Also, that way of processing the MD results allows the performance of a multilayer analysis by separating the structural components from each other. Good contrast is achieved for structural components of various sizes, which allows quantitative assessment of the molecular structure inside the unit cell. The outcome of the research may be useful in designing delivery vehicles for peptides and proteins.

It might be expected that this study will boost the development of a new Monte Carlo simulation method that could describe the thermodynamic parameters, e.g., chemical potential and free energy, relevant for insertion of cargo molecules into the H_{II} inverted hexagonal mesophase. Also, it

might inspire the researchers to perform more complex molecular dynamics simulations on H_{II} mesophases.

■ ASSOCIATED CONTENT

Supporting Information

Section S1: Constructing the simulation box (the unit cell); Section S2: Analysis of the local density dynamics; Section S3: Number of water molecules per headgroup; Section S4: Statistical distribution of the lattice parameter; periodic box dimensions (Table SI); selection recipe for the water molecules (Figure S1); chemical structure of a single GMO molecule (Figure S2); estimation of the GMO headgroup positions at the water/GMO interface (Figure S3); randomly generated two-dimension lattice within the hexagonal unit cell (Figure S4); representation of the supercell composed by repetition of the equilibrated H_{II} mesophase (Figure S5); Probability Mass Function of the lattice parameter (Figure S6); Distribution of the H-donor/H-acceptor distance of hydrogen bonds formed by the GMO headgroups and water (Figure S7). This material is available free of charge via the Internet at <http://pubs.acs.org>.

■ AUTHOR INFORMATION

Corresponding Author

*Mailing address: The Wolfson Department of Chemical Engineering, Technion, Technion City, Haifa 32000, Israel. E-mail: vlk@lcpe.uni-sofia.bg. Telephone number: +359 2 4891 229.

Notes

The authors declare no competing financial interest.

■ ACKNOWLEDGMENTS

Vesselin Kolev would like to acknowledge and extend his heartfelt gratitude to Technion for the provided partial fellowship. G. M. and A. I. are grateful to the FP7 project BeyondEverest.

■ REFERENCES

- Cherezov, V.; Clogston, J.; Papiz, M. Z.; Caffrey, M. Room to Move: Crystallizing Membrane Proteins in Swollen Lipidic Mesophases. *J. Mol. Biol.* **2006**, *357*, 1605–1618.
- Kulkarni, C. V.; Wachter, W.; Iglesias-Salto, G.; Engelskirchen, S.; Ahualli, S. Monoolein: A Magic Lipid? *Phys. Chem. Chem. Phys.* **2011**, *13*, 3004–3021.
- Yaghmur, A.; Laggner, P.; Zhang, S.; Rappolt, M. Tuning Curvature and Stability of Monoolein Bilayers by Designer Lipid-Like Peptide Surfactants. *PLoS One* **2007**, *e479*, 1–10.
- Mishraki, T.; Libster, D.; Aserin, A.; Garti, N. Temperature-Dependent Behavior of Lysozyme within the Reverse Hexagonal Mesophases (H_{II}). *Coll. Surf. B* **2010**, *75*, 391–397.
- Amar-Yuli, I.; Azulay, D.; Mishraki, T.; Aserin, A.; Garti, N. The Role of Glycerol and Phosphatidylcholine in Solubilizing and Enhancing Insulin Stability in Reverse Hexagonal Mesophases. *J. Colloid Interface Sci.* **2011**, *364*, 379–387.
- Luzzati, V.; Husson, F. The Structure of the Liquid-Crystalline Phases of Lipid-Water Systems. *J. Cell Biol.* **1962**, *12*, 207–219.
- Leikin, S.; Kozlov, M.; Fuller, N.; Rand, R. Measured Effects of Diacylglycerol on Structural and Elastic Properties of Phospholipid Membranes. *Biophys. J.* **1996**, *71*, 2623–2632.
- Templer, R.; Seddon, J.; Warrender, N.; Syrykh, A.; Huang, Z.; Winter, R.; Erbes, J. Inverse Bicontinuous Cubic Phases in 2:1 Fatty Acid/Phosphatidylcholine Mixtures. The Effects of Chain Length, Hydration, and Temperature. *J. Phys. Chem. B* **1998**, *102*, 7251–7261.
- Marsh, D. Pivotal Surfaces in Inverse Hexagonal and Cubic Phases of Phospholipids and Glycolipids. *Chem. Phys. Lipids* **2011**, *164*, 177–183.
- Hamm, M.; Kozlov, M. Tilt Model of Inverted Amphiphilic Mesophases. *Eur. Phys. J. B* **1998**, *6*, 519–528.
- Turner, D. C.; Gruner, S. M. X-ray Diffraction Reconstruction of the Inverted Hexagonal (H_{II}) Phase in Lipid-Water systems. *Biochemistry* **1992**, *31*, 1340–1355.
- Di Gregorio, G. M.; Mariani, P. Rigidity and Spontaneous Curvature of Lipidic Monolayers in the Presence of Trehalose: A Measurement in the DOPE Inverted Hexagonal Phase. *Eur. Biophys. J.* **2005**, *34*, 67–81.
- May, S.; Ben-Shaul, A. Molecular Theory of Lipid-Protein Interaction and the $L\alpha$ - H_{II} Transition. *Biophys. J.* **1999**, *76*, 751–767.
- May, S.; Kozlovsky, Y.; Ben-Shaul, A.; Kozlov, M. Tilt Modulus of a Lipid Monolayer. *Eur. Phys. J. E* **2004**, *14*, 299–308.
- Marrink, S.-J.; Tieleman, D. P. Molecular Dynamics Simulation of Spontaneous Membrane Fusion during a Cubic-Hexagonal Phase Transition. *Biophys. J.* **2002**, *83*, 2386–2392.
- Knecht, V.; Mark, A. E.; Marrink, S.-J. Phase Behavior of a Phospholipid/Fatty Acid/Water Mixture Studied in Atomic Detail. *J. Am. Chem. Soc.* **2006**, *128*, 2030–2034.
- Marrink, S.-J.; de Vries, A. H.; Mark, A. E. Coarse Grained Model for Semiquantitative Lipid Simulations. *J. Phys. Chem. B* **2004**, *108*, 750–760.
- Lee, W. B.; Mezzenga, R.; Fredrickson, G. H. Self-Consistent Field Theory for Lipid-Based Liquid Crystals: Hydrogen Bonding Effect. *J. Chem. Phys.* **2008**, *128* (074504), 1–10.
- Müller, M.; Schick, M. Calculation of the Phase Behavior of Lipids. *Phys. Rev. E* **1998**, *57*, 6973–6978.
- Nielsen, S. O.; Lopez, C. F.; Ivanov, I.; Moore, P. B.; Shelley, J. C.; Klein, M. L. Transmembrane Peptide-Induced Lipid Sorting and Mechanism of $L\alpha$ -to-Inverted Phase Transition Using Coarse-Grain Molecular Dynamics. *Biophys. J.* **2004**, *87*, 2107–2115.
- Li, X.-J.; Schick, M. Theory of Lipid Polymorphism: Application to Phosphatidylethanolamine and Phosphatidylserine. *Biophys. J.* **2000**, *78*, 34–46.
- Kolev, V.; Ivanova, A.; Madjarova, G.; Aserin, A.; Garti, N. Molecular Dynamics Approach to Water Structure of H_{II} Mesophase of Monoolein. *J. Chem. Phys.* **2012**, *136* (074509), 1–11.
- Mezzenga, R.; Meyer, C.; Servais, C.; Romoscanu, A.; Sagalowicz, L.; Hayward, R. Shear Rheology of Lyotropic Liquid Crystals: A Case Study. *Langmuir* **2005**, *21*, 3322–3333.
- Rand, R.; Fuller, N. Structural Dimensions and Their Changes in a Reentrant Hexagonal-Lamellar Transition of Phospholipids. *Biophys. J.* **1994**, *66*, 2127–2138.
- van der Spoel, D.; Lindahl, E.; Hess, B.; Groenhof, G.; Mark, A. E.; Berendsen, H. J. GROMACS: Fast, Flexible, and Free. *J. Comput. Chem.* **2005**, *26*, 1701–1718.
- (a) Klauda, J. B.; Brooks, B. R.; MacKerell, A. D.; Venable, R. M.; Pastor, R. W. An ab Initio Study on the Torsional Surface of Alkanes and Its Effect on Molecular Simulations of Alkanes and a DPPC Bilayer. *J. Phys. Chem. B* **2005**, *109*, 5300–5311. (b) Feller, S. E.; MacKerell, A. D. An Improved Empirical Potential Energy Function for Molecular Simulations of Phospholipids. *J. Phys. Chem. B* **2000**, *104*, 7510–7515.
- Jørgensen, W. L.; Chandrasekhar, J.; Madura, J. D.; Impey, R. W.; Klein, M. L. Comparison of Simple Potential Functions for Simulating Liquid Water. *J. Chem. Phys.* **1983**, *79* (926), 1–10.
- Jørgensen, W. L.; Madura, J. D. Temperature and Size Dependence for Monte Carlo Simulations of TIP4P Water. *Mol. Phys.* **1985**, *56*, 1381–1392.
- van Gunsteren, W. F.; Berendsen, H. J. C. *Groningen Molecular Simulation (GROMOS) Library Manual*; BIOMOS b.v.: Groningen, The Netherlands, 1987.
- Bussi, G.; Donadio, D.; Parrinello, M. Canonical Sampling through Velocity Rescaling. *J. Chem. Phys.* **2007**, *126* (014101), 1–7.
- Essmann, U.; Perera, L.; Berkowitz, M. L.; Darden, T.; Lee, H.; Pederson, L. A Smooth Particle Mesh Ewald Method. *J. Chem. Phys.* **1995**, *103* (8577), 1–17.

- (32) Miyamoto, Sh.; Kollman, P. Settle: An Analytical Version of the SHAKE and RATTLE Algorithm for Rigid Water Models. *J. Comput. Chem.* **1992**, *13*, 952–962.
- (33) Vega, C.; Abascal, J. L. F.; Conde, M. M.; Aragones, J. L. What Ice Can Teach Us about Water Interactions: A Critical Comparison of the Performance of Different Water Models. *Faraday Discuss.* **2009**, *141*, 251–276.
- (34) Probability distribution. In *Encyclopedia of Mathematics*; Hazewinkel, M., Ed.; Springer: Berlin, 2001.
- (35) Stare, J.; Mavri, J.; Grdadolnik, J.; Zidar, J.; Maksić, Z. B.; Vianello, R. Hydrogen Bond Dynamics of Histamine Monocation in Aqueous Solution: Car–Parrinello Molecular Dynamics and Vibrational Spectroscopy Study. *J. Phys. Chem. B* **2011**, *115*, 5999–6010.
- (36) Harper, P. E.; Mannock, D. A.; Lewis, R. N.; McElhaney, R. N.; Gruner, S. M. X-ray Diffraction Structures of some Phosphatidylethanolamine Lamellar and Inverted Hexagonal Phases. *Biophys. J.* **2001**, *81*, 2693–2706.
- (37) Rappolt, M.; Hodzic, A.; Sartori, B.; Ollivon, M.; Laggner, P. Conformational and Hydrational Properties during the L_β to L_α and L_α to H_{II} -Phase Transition in Phosphatidylethanolamine. *Chem. Phys. Lipids* **2008**, *154*, 46–55.
- (38) Perutkova, S.; Daniel, M.; Rappolt, M.; Pabst, G.; Dolinar, G.; Kralj-Iglic, V.; Iglic, A. Elastic Deformations in Hexagonal Phases Studied by Small-Angle X-ray Diffraction and Simulations. *Phys. Chem. Chem. Phys.* **2011**, *13*, 3100–3107.